Scale-invariant motion in intermittent chaotic systems

G. Zumofen
Laboratorium für Physikalische Chemie, Eidgenössische Technische Hochshule Zentrum, CH-8092 Zürich, Switzerland

J. Klafter
School of Chemistry, Tel-Aviv University, Tel-Aviv 69978, Israel
(Received 26 May 1992)

We investigate the dynamics generated from iterated maps and analyze the motion in terms of the probabilistic continuous-time random walk (CTRW) approach. Two different CTRW models are considered: (i) Particles jump between sites (turning points) or (ii) particles move at a constant velocity between sites and choose a new direction at random. For both models we study the mean-squared displacement $\langle r^2(t)\rangle$ and the propagator $P(r,t)$, the probability to be at location r at time t having started at the origin at $t=0$. Iterated maps are used to generate both dispersive and enhanced diffusion and the results are analyzed using the CTRW framework and scaling arguments. For the case of dispersive motion we discuss the problem of the stationary state and point out its relevance.

PACS number(s): 05.40.+j, 05.45.+b, 66.30.−h, 02.50.+s

I. INTRODUCTION

Diffusion processes are widespread and common in many fields in physics, chemistry, and biology and have therefore drawn the attention of both theorists and experimentalists. The diffusion process that has been most frequently encountered is the Brownian motion characterized by a mean-squared displacement that increases linearly with time, $\langle r^2(t)\rangle \sim t$, and by a Gaussian propagator $P(r,t)\sim t^{-d/2}\exp(-r^2/2t)$, where d is the spatial dimension in which Brownian particles diffuse.

Other laws of diffusion, slower and enhanced relative to the Brownian motion, have been recently under active investigations resulting in [1–6]

$$\langle r^2(t)\rangle \sim t^{\alpha}, \quad \alpha \neq 1 . \tag{1}$$

Cases with $\alpha<1$, known as the dispersive transport regime, have been attributed to random walks in geometrically disordered fractal structures or to temporal disorder, both having underlying scale-invariant properties, spatial or temporal with no characteristic length or time scales [1,2,7]. The $\alpha>1$ regime, which corresponds to enhanced diffusion, has been shown to originate from a number of models dominated by processes slowly decaying with time or with length [6,8,9]. One of these models, which accounts for the possibility of enhanced diffusion while still preserving a stochastic nature, is the Lévy walk model. Lévy walks are based essentially on a modification of the Lévy flights that display spatial scale invariance [10–12]. It has been established that both dispersive and enhanced motions have non-Gaussian propagators [6,13,14].

Parallel to these random-walk studies there has been considerable interest in nonlinear discrete maps, especially in the onset of chaotic behavior characterized by regular phases separated by intermittent bursts [15–18]. Interestingly both dispersive ($\alpha<1$) and enhanced ($\alpha>1$) diffusional behaviors have been recently observed in such maps under intermittent chaos [17–20]. It has been demonstrated [10,17,18,20,21] that one can relate the map-generated anomalous diffusion to random walks in continuous time. The mean-squared displacements obtained directly from the maps have excellent agreements with the random-walk analogous process in the dispersive and enhanced limits.

In this paper we extend the study of the maps beyond the mean-squared displacement and focus on the probability density $P(r,t)$ to be at r at time t, given an initial starting condition. We investigate these newly studied probability densities in the framework of the continuous-time random walks (CTRW) and confront our results with the map-generated probability densities.

The paper is organized as follows. In Sec. II we introduce the CTRW framework, which is applied later on two different diffusional limits. We define two approaches, the jump model and the velocity model, and compare them formally. In Sec. III we discuss the deterministic map of Geisel and Thomae [17], which leads to dispersive transport and use the CTRW jump model proposed in Ref. [17] to calculate the probability distribution $P(r,t)$. $P(r,t)$ is then compared directly with the map results. In Sec. IV a variant of the map in Sec. III is defined [18], this time leading to enhanced diffusion. The CTRW formulation is used again, suggesting a Lévy walk description of this map-generated motion. The jump model and the velocity model are analyzed and related to the map results. We end with a brief summary.

II. CONTINUOUS-TIME RANDOM-WALK MODELS

In this section we introduce the CTRW framework to be used in describing the map dynamics. We study sto-

chastic processes where particles can move either by waiting at a particular location before moving instantaneously to the next one (jump model), or by moving at a constant velocity between points of halt. We concentrate on the one-dimensional approach (generalization to higher dimensions is possible).

While the jump model has been extensively studied [1–8], the case of continuous motion with a given velocity has only lately received some attention and has therefore been studied to a much lesser extent [22,23]. In the constant velocity case one may distinguish between two different models. These two models do not lead to different characteristic behaviors and only differ in their analytical description: (i) Extending the regular random-walk approach, one may think of particles that move at a constant velocity for a given time (or displacement), then stop and choose a new direction and a new time of sojourn at random according to given probabilities. We call this the *velocity model.* (ii) If the particle proceeds its motion in the same direction the observer may not distinguish whether the particle has stopped at all or has simply continued its motion until it stops and changes direction. This leads to the picture that the particle moves at a constant velocity until it changes direction where the time between turning points is chosen at random. Following Masoliver, Lindenberg, and Weiss [24], we call this case the *two-state model.* In Fig. 1 we give a schematic description of the jump model and of the two cases of moving with a constant velocity between turning points.

In the CTRW framework the random-walk process is entirely specified by $\psi(r,t)$, the probability density to move a distance r in time t in a single motion event. $\psi(r,t)$ can be either decoupled $\psi(r,t)=\psi(t)\lambda(r)$, as commonly encountered in theories and applications of CTRW [1–7], or coupled through some space-time ansatz [10–12]. In the decoupled scheme, usually assumed in the jump model, $\psi(t)$ determines whether the motion is asymptotically regular or dispersive. The only requirement on $\lambda(r)$ is that its second moment is finite. In order to derive an enhanced diffusion behavior within the CTRW formulation, one has to introduce coupled memories [2,10]. Here we assume [8,10–12,25]

$$\psi(r,t)=p(r|t)\lambda(r) , \tag{2a}$$

$$p(r|t)=\delta(|r|-t) , \tag{2b}$$

where $p(r|t)$ is the conditional probability to move a distance r in time t. In the model studied here $p(r|t)$ is the δ function that accounts for the time delay necessary for the particle to move over the displacement r. For simplicity we introduce quantities given in units of length, time, and velocity. This space-time coupling scheme can now be introduced into the different models: jump, velocity, and two-state. While in the jump model no information is given on how the particle spends its time between jumps, the velocity picture with the coupled $\psi(r,t)$ of Eq. (2) provides a clear physical origin for spending the time between turning points by moving at constant velocity. Alternatively, one may rewrite Eq. (2) as

$$\psi(r,t)=\tfrac{1}{2}\delta(|r|-t)\psi(t) . \tag{3}$$

The two descriptions (2) and (3) are equivalent, i.e., the two expressions yield the same $\psi(r,t)$ if $\lambda(x)=\frac{1}{2}\psi(|x|)$.

In this paper we are mainly interested in the probability density $P(r,t)$ to be at location r at time t. We will calculate $P(r,t)$ in terms of $\psi(r,t)$ for the three models discussed above. In order to obtain $P(r,t)$ we define the probabilities $\Psi(t)$ and $\Psi(r,t)$ (note the difference between the ψ and Ψ notations). $\Psi(t)$, needed for the jump model, is the probability for not leaving a position up to time t [1,3]. This is related to $\psi(r,t)$ by

$$\Psi(t)=\int_t^\infty dt' \int dr\, \psi(r,t') . \tag{4}$$

Similarly, for the velocity model $\Psi(r,t)$ denotes the probability to pass at location r at time t in a single motion event; thus we may write [23]

$$\Psi(r,t)=p(r|t)\int_t^\infty dt' \int_{|r|}^\infty dr'\psi(r',t') . \tag{5}$$

By inserting (2b) or (3) into (5), we find for the coupled memory

$$\begin{aligned}\Psi(r,t)&=\delta(|r|-t)\int_{|r|}^\infty dr'\lambda(r')\\ &=\tfrac{1}{2}\delta(|r|-t)\int_t^\infty dt'\psi(t') .\end{aligned} \tag{6}$$

In order to derive recursive expressions for $P(r,t)$, we consider $Q(r,t)$, the probability to arrive at r exactly at time t and to stop before randomly choosing a new direction. Irrespective of which model we choose, the following recursive relation holds:

$$Q(r,t)=\int dr' \int_0^t dt' Q(r-r',t-t')\psi(r',t')+\delta(r)\delta(t) . \tag{7}$$

The propagator $P_J(r,t)$ for the *jump model* is then related to $Q(r,t)$ in the following way [1–3]:

$$P_J(r,t)=\int_0^t dt' Q(r,t-t')\Psi(t') . \tag{8}$$

Analogously, for the *velocity model* we assume that

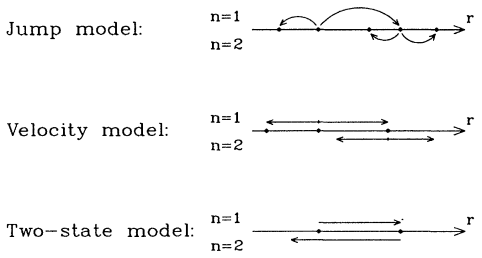

FIG. 1. Schematic representation of the three models of motion discussed in Sec. II. $n=1$ and $n=2$ denote two consecutive motion events. In the jump model the particle waits until it moves instantaneously to a new site. In the velocity model the particle moves at a constant velocity to a new site where it chooses a new direction at random, and in the two-state model the particle moves at a constant velocity between turning points where the intervals between turning points are chosen at random.

$P_V(r,t)$ is the probability to stop or pass at location r at time t and thus we have

$$P_V(r,t)=\int dr' \int_0^t dt' Q(r-r',t-t')\Psi(r',t') \ . \tag{9}$$

In the Fourier ($r\rightarrow k$) and Laplace ($t\rightarrow u$) spaces Eqs. (8) and (9) simplify to

$$P_J(k,u)=\Psi(u)/[1-\psi(k,u)] \tag{10}$$

and

$$P_V(k,u)=\Psi(k,u)/[1-\psi(k,u)] \ , \tag{11}$$

where we introduce for the Fourier and/or Laplace transforms the convention that the arguments indicate in which space the function is defined, e.g., $P(k,u)$ is the Fourier-Laplace transform of $P(r,t)$. For convenience we write the distribution $\psi(r,t)$ in Fourier-Laplace space as

$$\psi(k,u)=\tfrac{1}{2}[\psi_+(k,u)+\psi_-(k,u)] \tag{12}$$

with

$$\psi_\pm(k,u)=2\int_0^\infty dt \int_0^\infty dr \, e^{-r(u\pm ik)}\psi(r,t) \tag{13}$$

and in complete analogy $\Psi(k,u)$ in terms of $\Psi_\pm(k,u)$.

$\psi_\pm(k,u)$ and $\Psi_\pm(k,u)$ may be related to the quantities $h_\pm$ and $H_\pm$ in the two-state model of Masoliver, Lindenberg, and Weiss [24], where they correspond to probabilities of being in a left- or a right-moving state. For comparison we give the propagator of the two-state model

$$P_{\rm TS}(k,u)=\frac{\Psi_+(1+\psi_-)+\Psi_-(1+\psi_+)}{2(1-\psi_+\psi_-)} \ , \tag{14}$$

which differs from $P_V(k,u)$, Eq. (11). Obviously, the velocity model and the two-state model are closely related and in fact, there is a transformation so that for a given waiting-time distribution $\psi_V(r,t)$ there is a corresponding $\psi_{\rm TS}(r,t)$ such that $P_V(r,t)$ and $P_{\rm TS}(r,t)$ are identical. Considering for $\psi_V(r,t)$ the coupled memory approach Eq. (3), we write for the transformation

$$\psi_{\rm TS}(r,t)=\tfrac{1}{4}\delta(|r|-t)[\psi_V(t)+\tfrac{1}{2}\psi_V(t)\times\psi_V(t) +\tfrac{1}{4}\psi_V(t)\times\psi_V(t)\times\psi_V(t)+\cdots] \ , \tag{15}$$

where $\times$ denotes the convolution integration. Using the Laplace transformation Eq. (15) can be recast into

$$\psi_{\rm TS}(r,t)=\tfrac{1}{2}\delta(|r|-t)\mathcal{L}^{-1}\{\psi_V(u)/[2-\psi_V(u)]\} \ . \tag{16}$$

In general, no explicit expression can be derived for the transformation; however, for an exponential $\psi(t)$ or $\lambda(r)$ the transformation turns out to be simple. In this particular case we have

$$\psi(r,t)=\tfrac{1}{2}\delta(|r|-t)ae^{-at}=\delta(|r|-t)(a/2)e^{-ar} \ , \tag{17}$$

which in Fourier-Laplace space leads to

$$\psi_\pm(k,u)=a/(a+u\pm ik) \ , \tag{18a}$$

$$\Psi_\pm(k,u)=1/(a+u\pm ik) \ . \tag{18b}$$

Inserting Eqs. (18) into Eqs. (10) and (11) gives

$$P_J(k,u)=\frac{(a+u)^2+k^2}{(a+u)(au+u^2+k^2)} \tag{19}$$

and

$$P_V(k,u)=\frac{a+u}{au+u^2+k^2} \ . \tag{20}$$

Making use of Eq. (16) we obtain for the two-state model the following probability distribution:

$$\psi_{\rm TS}(r,t)=\tfrac{1}{2}\delta(|r|-t)(a/2)e^{-(a/2)t} \ , \tag{21}$$

which deviates from Eq. (17) by a constant only. If we insert Eq. (21) into Eqs. (12)–(14) we recover Eq. (20). This demonstrates that the velocity and the two-state model are related through the transformation of the corresponding waiting-time distributions. For a given jump rate the diffusion is faster by a factor of 2 in the velocity than in the two-state model, which reflects the fact that in the velocity model particles may continue their motion in the same direction when they stop to chose randomly a new direction.

Following the analysis in Ref. [24] we can relate the Eqs. (19) and (20) to partial differential equations. For the jump model we derive:

$$\frac{\partial^3 P_J}{\partial^3 t}+2a\frac{\partial^2 P_J}{\partial^2 t}+a^2\frac{\partial P_J}{\partial t}=a\frac{\partial^2 P_J}{\partial^2 r}+\frac{\partial^3 P_J}{\partial t\partial^2 r} \ , \tag{22}$$

while for $P_V(r,t)$ we obtain the telegrapher's equation

$$\frac{\partial^2 P_V}{\partial^2 t}+a\frac{\partial P_V}{\partial t}=\frac{\partial^2 P_V}{\partial^2 r} \ . \tag{23}$$

A discussion of the partial differential equation approach to anomalous diffusions as compared to the CTRW approach is given in Ref. [12]. In what follows we concentrate on two of the motion models only, the jump model and the velocity model (as depicted in Fig. 1), for which we calculate $P_J(r,t)$ and $P_V(r,t)$, respectively. The corresponding mean-square displacements are most easily presented in the Laplace space by

$$\langle r^2_{J,V}(u)\rangle=-\nabla_k^2 P_{J,V}(k,u)|_{k=0} \ , \tag{24}$$

which, using Eqs. (10) and (11), leads to

$$\langle r_J^2(u)\rangle=-\Psi(k,u)[1-\psi(k,u)]^{-2}\nabla_k^2\psi(k,u)|_{k=0} \tag{25}$$

and

$$\langle r_V^2(u)\rangle=-[1-\psi(k,u)]^{-1}\nabla_k^2\Psi(k,u)|_{k=0} -\Psi(k,u)[1-\psi(k,u)]^{-2}\nabla_k^2\psi(k,u)|_{k=0} \ . \tag{26}$$

An additional term appears in Eq. (26) when compared with Eq. (25). This term accounts for the fact that the particles move at a constant velocity and the diffusional motion may thus be more efficient for the velocity model than for the jump model.

III. DISPERSIVE MOTION

We start by introducing the iterated map studied by Geisel and Thomae [17], which has been shown to produce dispersive diffusion of the intermittent chaotic motion. For this type of motion we use the CTRW jump model in the description of the map results.

We denote the map by $g(x)$ and write for the nth iteration

$$x_{n+1}=g(x_n) . \tag{27}$$

Assuming periodic and inversion symmetries we have

$$g(x+N)=g(x)+N , \quad g(-x)=-g(x) , \tag{28}$$

where N is an integer and denotes the box number. With the help of these two rules the definition of the map is required only for the reduced range $0<x<\frac{1}{2}$. Following the formulation in Refs. [26,27], one may decompose the coordinate x of the trajectory into the box number N and the position $\tilde{x}$ within a box

$$x_n=N_n+\tilde{x}_n . \tag{29}$$

Thus the box number and the reduced coordinate $\tilde{x}$ have to be iterated individually:

$$\tilde{x}_{n+1}=\tilde{g}(\tilde{x}_n) , \quad 0<\tilde{x}<1 , \tag{30a}$$

$$N_{n+1}=\hat{g}(\tilde{x}_n)+N_n , \tag{30b}$$

where $\tilde{g}(\tilde{x})$ is the reduced map for the reduced coordinate $\tilde{x}$ and $\hat{g}(\tilde{x})$ is used to increment or decrement the box number N.

For the displacement $r(t)$ after t iterations, we have

$$r(t)=x_{n+t}-x_n , \tag{31}$$

with the initial coordinate x_0 chosen arbitrarily. Here we are confronted with the problem of how to choose n as the origin of the observation. Interestingly, this relates the problem of determining the origin to that of the stationary states in CTRW and will be discussed at the end of the section. The propagator $P(r,t)$ is calculated according to

$$P(r,t)=\langle \delta(r-N_{n+t}+N_n)\rangle , \tag{32}$$

where the average is taken over a set of initial iterations $\{n\}$. In Eq. (32) $P(r,t)$ is defined for integer values of r.

Geisel and Thomae [17] considered the following type of map:

$$g(x)=\begin{cases}(1+\epsilon)x+ax^z , & 0\le x<x_c \\ \dfrac{3}{2}-\dfrac{|4x-1-2x_c|}{1-2x_c} , & x_c\le x\le\frac{1}{2} ,\end{cases} \tag{33}$$

which represents a combination of a nonlinear and piecewise linear branches. The quantity ϵ in Eq. (33) is considered as a control parameter to prevent the iteration process from remaining in laminar stage beyond the typical time of observation. The map in Eq. (33) has been shown to generate dispersive motion, namely the mean-squared displacement grows sublinearly with time [17].

For our purpose we restrict the map function to the nonlinear branch and enlarge its range of validity, so that

$$g(x)=(1+\epsilon)x+ax^z , \quad 0\le x<\tfrac{1}{2} . \tag{34}$$

We choose the constant to be $a=2^z(1-\epsilon/2)$. Actually, we obtained better agreement between the simulation of the iterative process and the CTRW approach when using the map in Eq. (34) compared to the one in Eq. (33). Moreover, we prefer this representation because of its close resemblance to the map we are going to use (in the next section) for the enhanced motion. In Fig. 2 we present the map $g(x)$ over the range of three boxes. The translational and mirror symmetries are evident from the figure. In Fig. 3 we show the reduced map $\tilde{g}(x)$, and indicate the ranges of the branches from which the box number N is incremented or decremented.

Already Geisel and Thomae [17] proposed the CTRW approach as a description of the time evolution of the mean-squared displacements. Following this proposal, we assume a decoupled $\psi(r,t)$ and consider the waiting-time distribution as the probability distribution of the particle to stay in a laminar stage. We adopt the notation introduced in Ref. [17] and write for this distribution:

$$\psi(t)=\frac{2(2^{z-1}\epsilon+a)e^{\epsilon(z-1)t}}{[(2^{z-1}+a/\epsilon)e^{\epsilon(z-1)t}-a/\epsilon]^{z/(z-1)}} , \tag{35}$$

which for $\lim\epsilon\to 0$ is

$$\psi(t)=2a/[2^{z-1}+a(z-1)t]^{z/(z-1)} . \tag{36}$$

Expressions (35) and (36) have a power-law dependence for long times $\psi(t)\sim t^{-z/(z-1)}$. For the purpose of our analysis we use

$$\psi(t)=\gamma/[1+t]^{\gamma+1} , \tag{37}$$

where we set $\gamma=1/(z-1)$. The Laplace transformation can be calculated analytically:

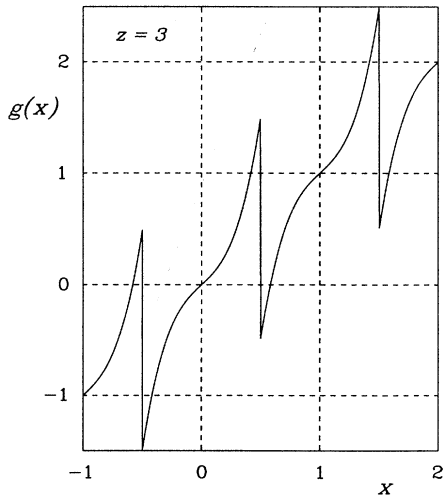

FIG. 2. Map $g(x)$ for the dispersive motion Eq. (34) for $z=3$. The discontinuities for $x\simeq\frac{1}{2}+N$ and the tangent contact to the diagonal for $|x-N|\simeq 0$ should be noted.

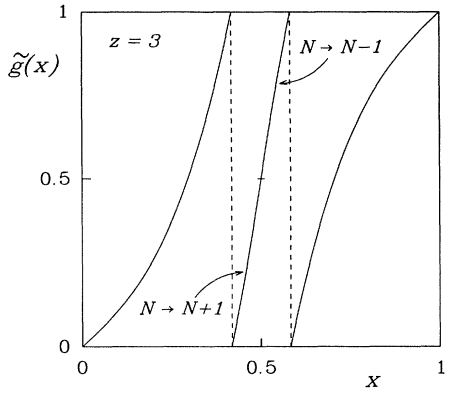

FIG. 3. Reduced map $\tilde{g}(x)$ for the dispersive motion Eq. (30) for $z=3$. The lower and the upper halves of the central branch are associated with an increment and a decrement of the cell number N, respectively.

$$\psi(u)=\begin{cases}\gamma u^{\gamma}e^{u}\Gamma(-\gamma,u)\ , & \gamma\neq 1,2,\ldots \\ 1-ue^{u}E_1(u)\ , & \gamma=1\ ,\end{cases} \tag{38}$$

where $\Gamma(\alpha,x)$ denotes the incomplete γ function and $E_1(x)$ is the exponential integral. For small u values we have the expansion

$$\psi(u)\sim\begin{cases}1-cu^{\gamma}\ , & 0<\gamma<1 \\ 1+u\ln(u)\ , & \gamma=1 \\ 1-\bar{t}u-cu^{\gamma}\ , & 1<\gamma<2\ ,\end{cases} \tag{39}$$

where $c=\Gamma(1-\gamma)$ and the mean waiting time $\bar{t}=(\gamma-1)^{-1}$, respectively. The third regime $1<\gamma<2$ can be extended to cover also $\gamma>2$ but with integer powers of u smaller than γ. Note that in the range $0<\gamma<1$, which corresponds to $z>2$, $\psi(t)$ has no finite moment and therefore the random-walk process has no characteristic time that leads naturally to dispersive diffusion [1]. Only in the range $\gamma>1$, namely, $1<z<2$, does a characteristic time $\bar{t}$ exist.

For the space part of the probability distribution $\lambda(r)$ we assume that there is a typical step length per iteration, which we set to unity $\lambda(r)=\frac{1}{2}\delta(|r|-1)$. The Fourier transform then simply is

$$\lambda(k)=\cos k\ . \tag{40}$$

Inserting Eqs. (39) and (40) into Eq. (24), we obtain the asymptotic expressions for the mean-squared displacements

$$\langle r^2(t)\rangle\sim\begin{cases}t^{\gamma}\ , & 0<\gamma<1 \\ t/\ln t\ , & \gamma=1 \\ t\ , & 1<\gamma\ ,\end{cases} \tag{41}$$

which, as demonstrated in Ref. [17], agree well with the mean-squared displacements obtained directly from the iterated maps.

Here we go beyond the mean-squared displacement calculations and analyze the corresponding propagators (whose second moments are the mean-squared displacements). We still stay with a decoupled memory and restrict our derivations to that of the jump model. Taking the Fourier back transform of expression (10), we obtain

$$P_J(r,u)=\frac{1-\psi(u)}{2\pi u}\int_{-\pi}^{\pi}dk\frac{e^{ikr}}{1-\psi(u)\cos k}\ , \tag{42}$$

where we have made use of the relation $\Psi(u)=[1-\psi(u)]/u$. For integer r values the integration yields

$$P_J(r,u)=\frac{1}{u}\left[\frac{1-\psi(u)}{1+\psi(u)}\right]^{1/2}V^{|r|}(u)\ , \tag{43}$$

where

$$V(u)=\frac{1}{\psi(u)}\{1-[1-\psi^2(u)]^{1/2}\}\ . \tag{44}$$

We concentrate on the dispersive case with $0<\gamma<1$ and derive the asymptotic forms of $P_J(r,t)$, considering the long-time (small u) behavior. First we present the autocorrelation function, which we denote by $P_0(t)=P(r=0,t)$, the probability distribution to stay at the origin

$$P_0(u)=\frac{1}{u}\left[\frac{1-\psi(u)}{1+\psi(u)}\right]^{1/2}\simeq(c/2)^{1/2}u^{\gamma/2-1}\ . \tag{45}$$

Laplace inversion gives

$$P_0(t)=a_0/t^{\gamma/2}\ ,\quad 0<\gamma<1\ , \tag{46}$$

with

$$a_0=[\Gamma(1-\gamma)/2]^{1/2}/\Gamma(1-\gamma/2)\ . \tag{47}$$

To obtain approximate forms for the r dependence of $P_J(r,t)$ we consider the following approximation, which holds for small u values:

$$\begin{aligned}P_J(r,u)&=\frac{1}{u}\left[\frac{1-\psi(u)}{1+\psi(u)}\right]^{1/2}\exp[|r|\ln V(u)] \\ &\simeq[\Gamma(1-\gamma)/2]^{1/2}u^{\gamma/2-1}\exp[-|r|(2cu^{\gamma})^{1/2}]\ .\end{aligned} \tag{48}$$

The relationship between r and u in the exponent indicates that there is a scaling behavior. For small r we consider a second-order expansion of (48):

$$P_J(r,u)\simeq P_0(u)[1-(2cu^{\gamma})^{1/2}|r|+cu^{\gamma}r^2]\ , \tag{49}$$

which under Laplace inversion gives

$$\begin{aligned}P_J(r,t)\simeq{}&a_0t^{-\gamma/2}-c|r|/[\Gamma(1-\gamma)t^{\gamma}] \\ &+(c^3/2)^{1/2}r^2/[\Gamma(1-3\gamma/2)t^{3\gamma/2}]\ .\end{aligned} \tag{50}$$

Considering a second-order cumulant approximation for $P_J(r,t)$, Eq. (50) can be recast into

$$P_J(r,t)\simeq a_0t^{-\gamma/2}\exp(-a_1\xi-a_2\xi^2)\ , \tag{51}$$

where we introduced the scaling variable $\xi=|r|/t^{\gamma/2}$.

The constants are

$$a_1 = a_0^{-1} \tag{52a}$$

and

$$a_2 = a_1^2/2 - \Gamma(1-\gamma)\Gamma(1-\gamma/2)/\Gamma(1-3\gamma/2) \; . \tag{52b}$$

For large r we follow the derivation by Weiss and coworkers [13] using a steepest-descent approximation to expression (48), which leads to the scaling form

$$P_J(r,t) \simeq b_0 t^{-\gamma/2} \xi^{\beta} \exp(-b_1 \xi^{\nu}) \tag{53}$$

with

$$\beta = (\gamma-1)/(2-\gamma) \; , \quad \nu = 2/(2-\gamma) \tag{54}$$

and

$$b_0 = \frac{1}{2} \left[\frac{[\Gamma(1-\gamma)]^{1+\beta}}{\pi(1-\gamma/2)2^{\beta}} \right]^{1/2} \gamma^{\beta} \; ,$$

$$b_1 = \gamma^{\nu} [\Gamma(1-\gamma)/2]^{\nu/2} \left[\frac{2}{\gamma} - 1 \right] \; . \tag{55}$$

Obviously, Eqs. (51) and (53) can be rewritten as

$$P_J(r,t) \sim t^{-\gamma/2} f(\xi) \; , \tag{56}$$

where $f(\xi)$ is the scaling function

$$f(\xi) \simeq \begin{cases} e^{-a_1\xi - a_2\xi^2} \; , & \text{for small } \xi \\ \xi^{\beta} e^{-b_1 \xi^{\nu}} \; , & \text{for large } \xi \; . \end{cases} \tag{57}$$

Recall here the scaling variable is $\xi = |r|/t^{\gamma/2}$. Higher-order terms can also be calculated from the short- and the long-range expressions of $f(\xi)$. Figs. 4 and 5 demonstrate the two ξ regimes described in Eqs. (56) and (57). Shown is $P(r,t)$ for $\gamma = \frac{1}{2}$ ($z = 3$) as a function of the scaling variable ξ. Full lines give exact results obtained from a numerical Laplace inversion of Eq. (43) for various times t. In Fig. 4 we clearly observe a cusp of $P(r,t)$ at the origin. In Fig. 5 the convergence of the curves to the asymptotic form is obvious. The broken lines show the two approximate limits in Eq. (57). Good agreement is obeyed for both small and large ξ, respectively.

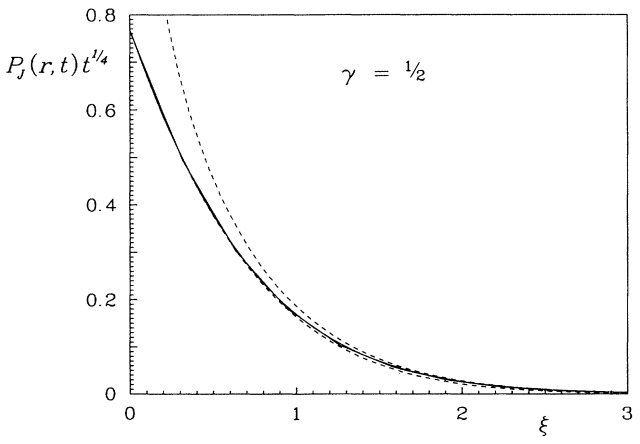

FIG. 4. Propagator $P_J(r,t)$ for the dispersive motion in the jump model. The full lines denote the exact results obtained from a numerical Laplace inversion of Eq. (43) for $\gamma = \frac{1}{2}$ and for times $t = 10^2$, 10^4, and 10^6. The scaling variable is $\xi = r/t^{1/4}$. The dashed lines denote the asymptotic approximations Eqs. (51) and (52) for small ξ and for large ξ, respectively.

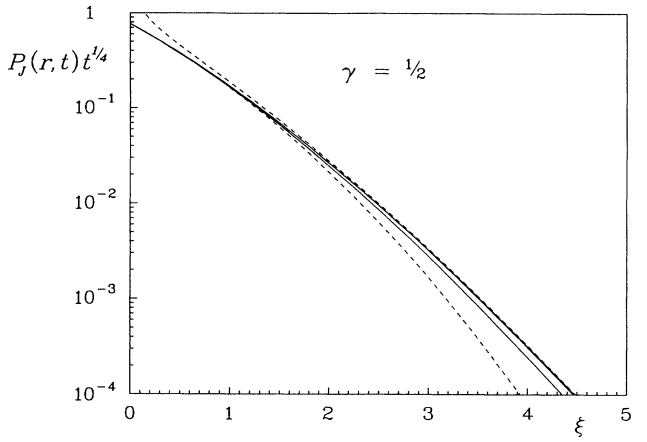

FIG. 5. Same as in Fig. 4 but on logarithmic vs linear scales. Note the convergence of the curves with increasing time t to the limiting asymptotic form.

It has been shown that iterations of the map of the type Eq. (33) lead to a laminar behavior where particles remain for a large number of iterations almost at the same location followed by a period during which the box number changes. As mentioned above this raises the questions of how to choose an iteration as the beginning of observation. For a choice of any iteration, i.e., iteration in the chaotic or laminar stage, we are in the stationary-state condition that was studied in the CTRW context [28,29]. It was pointed out that the very first step of a process can give rise to some changes. This is in fact the case for iterated maps and for their corresponding CTRW's. If one chooses an iteration during the chaotic motion, then we believe that the injection into the laminar phase samples the typical waiting-time distribution and that in this way the first step follows the distribution, which is identical for all consecutive steps. This is the situation encountered in usual CTRW analyses and does not lead to the problem of the stationary state, as discussed below. For the criterion of an iteration step n to be in the chaotic regime we consider the inequality $|x_{n+1} - x_n| > \frac{1}{2}$ and apply this criterion for the determination of the set $\{n\}$ over which the average is calculated in Eq. (32).

The propagator obtained from the iterated map according to this averaging is shown in Fig. 6 for various times t. 10^{10} number of iterations were performed and the parameter ϵ was set to $\epsilon = 10^{-6}$. The resolution in the histogram was chosen to be of unity. The convergence to the limiting asymptotic form is apparent as it is in Fig. 5 for the CTRW approach. The dashed line denotes the theoretical curve taken from Fig. 5 but rescaled by a factor of 1.08, a value considered as a free

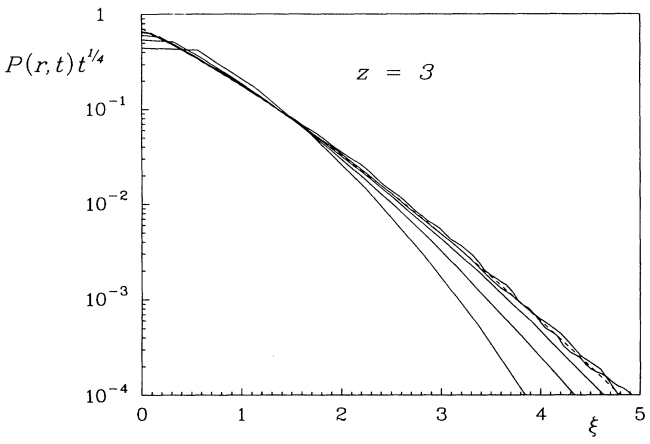

FIG. 6. Propagator $P(r,t)$ obtained from the iterated map Eq. (34) for $z=3$, which corresponds to $\gamma=\frac{1}{2}$. Full lines denote the map results for times $t=10$, 10^2, 10^3, and 10^4. The convergence to the limiting form with increasing time is apparent. The scaling variable is $\xi=r/t^{1/4}$. The dashed line is the rescaled theoretical result for $t=10^4$ taken from Fig. 5.

parameter to account for the different prefactors in Eqs. (36) and (38) and for an effective stepping length.

The problem of the stationary state was introduced by Feller [28] and discussed later by Tunaley [29] and concerns the question how the observations change when the time origin of the observation differs from that of the initiation of the transport process. We adopt the equation presented in Ref. [5] for a stationary condition

$$P^{\rm eq}(k,u)=\frac{1-h(u)+\lambda(k)[h(u)-\psi(u)]}{u[1-\psi(u)\lambda(k)]} , \tag{58}$$

where $h(t)$ denotes the probability distribution of the first step

$$h(u)=\Psi(u)/\bar{t} . \tag{59}$$

Apparently, we notice that only for a finite mean waiting time expression (59) is relevant and therefore we concentrate on the regime $1<\gamma<2$ [see Eq. (39)]. To simplify the Fourier back transformation we rewrite Eq. (58) as

$$P^{\rm eq}(k,u)=\frac{h(u)[1-\psi(u)]}{u\psi(u)[1-\psi(u)\lambda(k)]}+\frac{[\psi(u)-h(u)]}{u\psi(u)} . \tag{60}$$

Taking the Fourier back transform of Eq. (60) the second term on the right-hand side (rhs) leads to a δ_r contribution, which gives rise to a peak at the origin. The first term can be evaluated according to Eqs. (42)–(44). The integration then yields

$$P^{\rm eq}(r,u)=\frac{h(u)[1-\psi(u)]^{1/2}}{u\psi(u)[1-\psi(u)]^{1/2}}V^{|r|}(u)+\delta_r\frac{\psi(u)-h(u)}{u\psi(u)} , \tag{61}$$

where $V(u)$ is the quantity given in Eq. (44). Equation (61) is still exact, and we apply it for the computation of $P^{\rm eq}(r,t)$ using a numerical Laplace inversion procedure.

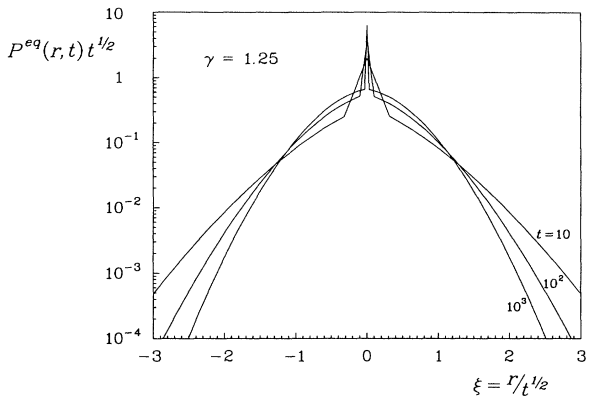

FIG. 7. Stationary state propagator $P^{\rm eq}(r,t)$ obtained from the numerical Laplace inversion of Eq. (61) for $\gamma=\frac{5}{4}$. The times chosen are as indicated. Note the convergence of the curves to the asymptotic behavior of the regular diffusion except for the peak at the origin which is due to the anomalous pausing-time distribution of the first step.

To derive the long-time asymptotic forms one may insert the small u approximations of $\psi(u)$, Eq. (39), into Eq. (59), which yields

$$h(u)\simeq 1+cu^{\gamma-1}/\bar{t}=1-\Gamma(2-\gamma)u^{\gamma-1} . \tag{62}$$

For the propagator we thus have

$$P^{\rm eq}(r,u)\simeq\frac{\bar{t}}{2\pi}\int_{-\pi}^{\pi}\frac{e^{ikr}}{\bar{t}u+k^2/2}dk+\delta_r\Gamma(2-\gamma)u^{\gamma-2} , \tag{63}$$

where cos$k$ in the denominator was expanded to second order. The first term on the rhs indicates regular diffusion, so that,

$$P^{\rm eq}(r,t)\simeq(\bar{t}/2\pi t)^{1/2}\exp(-r^2\bar{t}/2t)+\delta_r t^{1-\gamma} . \tag{64}$$

In Fig. 7 we present the numerical results obtained from

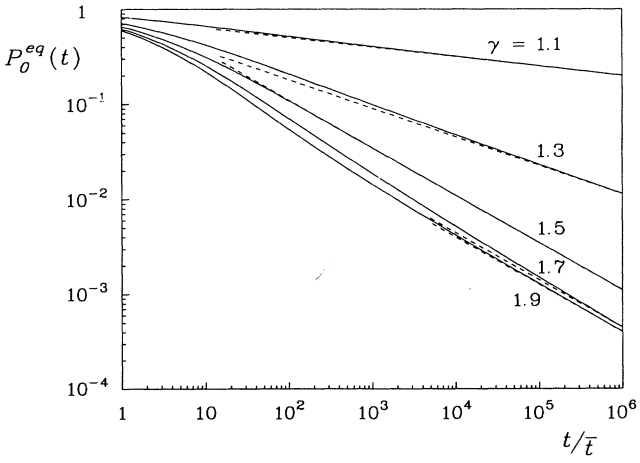

FIG. 8. Stationary-state autocorrelation function $P_0^{\rm eq}(t)$. Full lines give the exact result obtained from a numerical Laplace inversion of Eq. (61) for various γ values as indicated. The dashed lines denote the predicted asymptotic slopes according to Eq. (65).

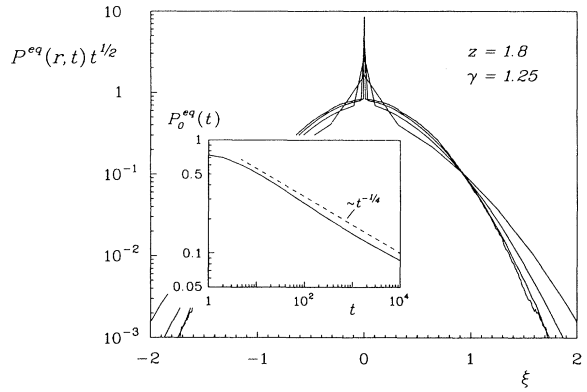

FIG. 9. Stationary-state propagator $P^{eq}(r,t)$ obtained from the iterated map Eq. (34) for $z=1.8$, which corresponds to $\gamma=\frac{5}{4}$ and for times $t=10$, 10^2, 10^3, and 10^4. Note the convergence of the curves to the asymptotic behavior of the regular diffusion with increasing time except for the peak at the origin, similarly as obtained from the CTRW approach Fig. 7. The scaling variable is $\xi=r/t^{1/2}$. In the insert the full line gives the autocorrelation function $P_0^{eq}(t)$ (the decay at the origin). The dashed line denotes the predicted asymptotic slope.

the numerical Laplace inversion of Eq. (61) for various times t. The curves are plotted as a function of the scaling variable $\xi=r/t^{1/2}$ resulting from the first term on the rhs of Eq. (64). The second term dominates the behavior at the origin.

In Fig. 8 we show the autocorrelation function $P_0^{eq}(t)$ for several γ values in the range $1<\gamma<2$. In the reduced range $1<\gamma<\frac{3}{2}$ the behavior of $P_0^{eq}(t)$ is governed by the second term of the rhs of Eq. (64) while for $\gamma>\frac{3}{2}$ the first term dominates following

$$P_0^{eq}(t)\sim\begin{cases} t^{1-\gamma}\ , & 1<\gamma<\frac{3}{2} \\ \\ t^{-1/2}\ , & \frac{3}{2}<\gamma \end{cases} \quad \text{for large } t\ . \tag{65}$$

Figure 9 shows $P^{eq}(r,t)$ obtained from the iterated map Eq. (34) for $z=1.8$ corresponding to $\gamma=1.25$ and for various times t. Here the average was taken over all n values in Eq. (32) in contrast to the set $\{n\}$ used in the calculations presented in Fig. 6 and ϵ was set to zero. There is a good qualitative agreement with the results of Fig. 7. The insert gives $P_0^{eq}(t)$ as a function of time, which for longer times follows the predicted decay of $t^{-1/4}$.

IV. ENHANCED DIFFUSION

In this section we study enhanced diffusion as obtained from iterated maps. This time we analyze the results in terms of the CTRW approach with coupled $\psi(r,t)$ and relate the subsequent derivations to previous works on Lévy walks [10–12,14]. Here we return to a comparison between the jump model and velocity model.

We again follow a map studied by Geisel, Nierwetberg, and Zacherl, 18], which generates enhanced diffusion in intermittent chaotic motion. This map is closely related to that given in Eq. (34). For the reduced range the definition is

$$g(x)=(1+\epsilon)x+ax^z-1\ ,\quad 0\le x\le\tfrac{1}{2}\ , \tag{66}$$

where a is set to $a=2^z(1-\epsilon/2)$. In contrast to the map in Eq. (34) the map in Eq. (66) is discontinuous at the cell boundaries. Figs. 10 and 11 are analogous to Figs. 2 and 3 and show the map of Eq. (66) over three cells and a reduced map, respectively.

As pointed out in Ref. [18] the intermittent behavior of the two maps in Eqs. (34) and (66) is equivalent. However, in Eq. (66) the laminar phase is associated with steps of approximately a cell unit per iteration. Thus, one may assume that during the laminar phase the particle moves at a constant velocity. Guided by this assumption Geisel, Nierwetberg, and Zacherl [18] calculated a velocity-velocity correlation function using the probability distribution for staying in a laminar phase. From this correlation function they could derive asymptotic forms for the mean-squared displacement. Here, in order to calculate the propagator we apply the space-time coupled memory function of Eq. (3) and write

$$\psi(r,t)=\frac{(2^{z-1}\epsilon+a)e^{\epsilon(z-1)t}}{[(2^{z-1}+a/\epsilon)e^{\epsilon(z-1)t}-a/\epsilon]^{z/(z-1)}}\delta(|r|-t)\ , \tag{67}$$

where the δ function accounts for the motion in the laminar phase. We note that apart from the δ function correlation the distribution $\psi(r,t)$ in Eq. (67) is similar to the one in Eq. (35), which gave rise to dispersive motion.

For the purpose of applying the CTRW we make use of our derivations in Refs. [14,25] where the Lévy walk con-

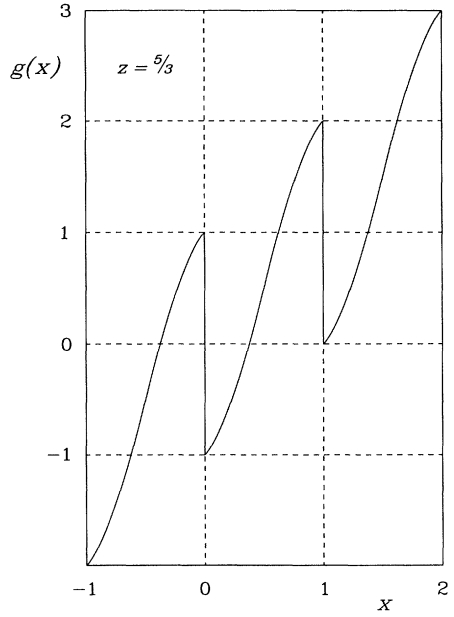

FIG. 10. Map $g(x)$ for the enhanced diffusion Eq. (66) for $z=\frac{5}{3}$. Note the discontinuities for $x\simeq N$ and the tangent contact $x_{n+1}=x_n\pm1$ for $x\simeq N$.

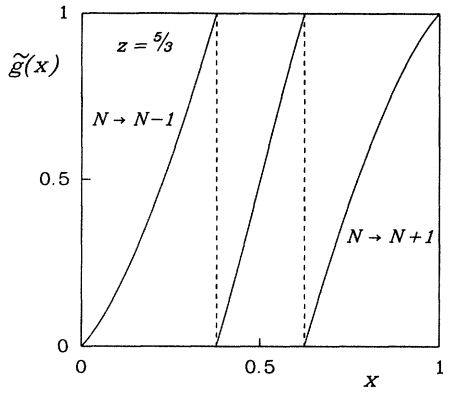

FIG. 11. Reduced map $\tilde{g}(x)$ for the enhanced diffusion and for $z=\frac{5}{3}$. The branches on the left and on the right are associated with a decrement and an increment of the cell number N, respectively.

cept was considered within the framework of the jump model with a coupled memory approach, which has a spatial power-law dependence. Equation (67) shows a temporal power-law dependence. However, as shown in Sec. II there is no difference between the two ways of describing $\psi(r,t)$, Eqs. (2) and (3). We thus rewrite the coupled memory as

$$\psi(r,t)=\tfrac{1}{2}A\delta(|r|-t)|r|^{-\mu}\ , \quad r\neq 0\ , \tag{68}$$

where we considered a discrete lattice with integer values of r. The constant A accounts for the normalization $A^{-1}=\zeta(\mu)$, where ζ denotes the Riemann zeta function. Comparing Eqs. (67) and (68) we relate the two exponents μ and z to each other: $\mu\equiv z/(z-1)$.

Fig. 12 demonstrates the probability densities $\psi(t)$ and

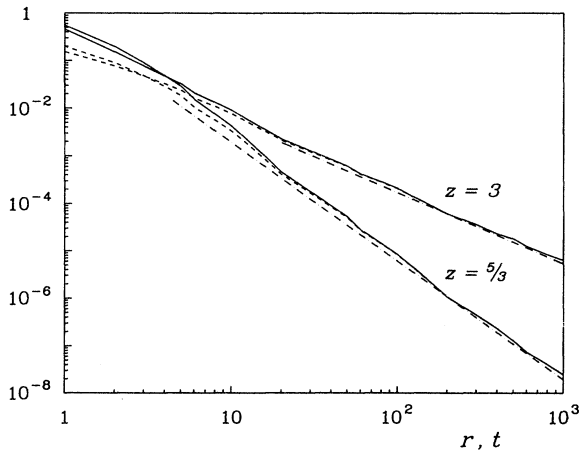

FIG. 12. Stepping probability distributions obtained from the iterated map, Eq. (66) for $z=3$ and $z=\frac{5}{3}$. The full lines give the waiting-time distribution $\psi(t)$ and the dashed lines denote the corresponding stepping-length distribution $2\psi(r)$. The dash-dotted lines give the theoretical slopes of 1.5 and 2.5 for $z=3$ and $z=\frac{5}{3}$, respectively.

$\psi(r)$ obtained directly from the map Eq. (66). Asymptotically, the two distributions $\psi(t)$ and $2\psi(r)$ fall on top of each other, which supports the δ function introduced in Eq. (67) to account for the space-time coupling. To guarantee that the first step of a motion event starts from a chaotic phase we used the inequality $|x_{n+1}-x_n|<\frac{1}{2}$, which differs from the criterion applied for the dispersive motion by inverting the inequality from larger than $\frac{1}{2}$ to smaller than $\frac{1}{2}$.

For the Fourier-Laplace transform of $\psi(r,t)$ we choose the form

$$\psi(k,u)=\tfrac{1}{2}[\phi(q)+\phi(\bar{q})]\ , \tag{69}$$

with $q=u+ik$ and $\bar{q}=u-ik$ and with

$$\phi(q)=A\sum_{r(>0)} e^{-qr}r^{-\mu}\ . \tag{70}$$

To obtain an expansion for small values of q we consider a decomposition by adding and subtracting terms:

$$\begin{aligned}\phi(q)=A\sum_{r(>0)} r^{-\mu}&\left[e^{-rq}-1+rq-\cdots-\frac{(-1)^n}{n!}(rq)^n\right]\\&+A\sum_{r(>0)} r^{-\mu}-qA\sum_{r(>0)} r^{1-\mu}+\cdots\\&+\frac{(-1)^n}{n!}q^nA\sum_{r(>0)} r^{n-\mu}\ ,\end{aligned} \tag{71}$$

where n is the largest integer smaller than $\mu-1$ and, for integer μ, $n=\mu-2$. We now replace the sum in the first term in Eq. (71) by an integral and obtain the Saalschütz form, for which we have [14]

$$\phi(q)\simeq\begin{cases}1+c_\mu q^{\mu-1}\ , & 1<\mu<2\\ 1-c_1q+c_\mu q^{\mu-1}\ , & 2<\mu<3\\ 1-c_1q+c_2q^2+c_\mu q^{\mu-1}\ , & 3<\mu<4\ .\end{cases} \tag{72}$$

For integer subscripts the constants are $c_j=\zeta(\mu-j)/[j!\zeta(\mu)]$ and otherwise $c_\mu=\Gamma(1-\mu)/\zeta(\mu)$. c_1 corresponds to the mean waiting time $c_1=\bar{t}=\zeta(\mu-1)/\zeta(\mu)$. For $\mu=2$ we again replace the first sum in (71) by an integral which by partial integration leads to

$$\phi(q)\simeq 1-q\int_1^\infty dr r^{-1}e^{-qr}\ , \tag{73}$$

where we have introduced the lower integration limit of 1 to avoid divergence. We proceed in an analogous way for $\mu=3$ and obtain to lowest order

$$\phi(q)\simeq\begin{cases}1+q\ln q\ , & \mu=2\\ 1-c_1q-q^2\ln q\ , & \mu=3\ ,\end{cases} \tag{74}$$

where c_1 is again the mean waiting time $c_1=\bar{t}=\zeta(2)/\zeta(3)$. We now link $\Psi(k,u)$ from Eq. (5) to $\phi(q)$ through

$$\Psi(k,u)=(A/2)\sum_{r(>0)}(e^{-qr}+e^{-\bar{q}r})\sum_{j(\geq r)} j^{-\mu}\ , \tag{75}$$

and by approximating the sums in Eq. (75) by integrals, we obtain

$$\Psi(k,u)\simeq\tfrac{1}{2}\int_{\eta}^{\infty}dr(e^{-qr}+e^{-\bar{q}r})(1-A\int_{\eta}^{r}dx\,x^{-\mu})$$
$$\simeq\frac{1}{2q}[1-\phi(q)]+\frac{1}{2\bar{q}}[1-\phi(\bar{q})]\ , \tag{76}$$

where η denotes a lower bound cutoff. From expression (76) we notice that

$$\Psi(u)=\Psi(k=0,u)=\frac{1}{u}[1-\psi(u)]\ , \tag{77}$$

which is the familiar relationship that ultimately relates the expressions (10) and (11) for the jump and velocity models.

To calculate the mean-squared displacement we make use of Eqs. (25) and (26) and find to leading order that

$$\langle r^2_{J,V}(t)\rangle\sim\begin{cases}t^2\ , & 1<\mu<2\\ t^2/\ln t\ , & \mu=2\\ t^{4-\mu}\ , & 2<\mu<3\\ t\ln(t)\ , & \mu=3\\ t\ , & 3<\mu\ .\end{cases} \tag{78}$$

Interestingly, the two expressions (25) and (26) follow, to leading order, the same behavior, which means that quantitatively the diffusion may be faster in the velocity model than in the jump model, but qualitatively both models show the same behavior. The results of Eq. (78) have been previously derived by Geisel, Nierwetberg, and Zacherl [18].

We again extend the study and investigate the propagators $P(r,t)$ for the enhanced regime. We follow our derivations in Ref. [14] and begin with the regime $1<\mu<2$, which exhibits ballistic-type motion. In the jump model to lowest order in u and k we have

$$P_J(k,u)\simeq c_\mu u^{\mu-2}/[c_\mu u^{\mu-1}+\tilde{c}|k|^{\mu-1}]\ ,\quad 1<\mu<2\ , \tag{79}$$

where $\tilde{c}=c_\mu\cos[\pi(\mu-1)/2]$. The Fourier-Laplace back transformation leads to

$$P_J(r,t)\simeq\begin{cases}bt^{-1}(t/r)^{2-\mu}\ , & r<t\\ 0\ , & r>t\ ,\end{cases} \tag{80}$$

with

$$b=-\cot(\pi\mu/2)/\pi\ .$$

This result differs from the expression in the velocity picture, where we obtain

$$P_V(k,u)\simeq\frac{q^{\mu-2}+\bar{q}^{\mu-2}}{q^{\mu-1}+\bar{q}^{\mu-1}}\ . \tag{81}$$

We do not investigate this form in detail. There is, however, an analytical expression of $P_V(r,t)$ for $\mu=\frac{3}{2}$, which may be taken as a representative form for the $1<\mu<2$ range. For $\mu=\frac{3}{2}$ expression (81) simplifies to

$$P_V(k,u)\simeq(q^{-1/2}+\bar{q}^{-1/2})(q^{1/2}+\bar{q}^{1/2})^{-1}$$
$$=(q\bar{q})^{-1/2}=(u^2+k^2)^{-1/2}\ , \tag{82}$$

which, upon Fourier inversion, is

$$P_V(r,u)\simeq\tfrac{1}{2}K_0(ru)\ , \tag{83}$$

where K_0 is a modified Bessel function. The Laplace inversion then gives

$$P_V(r,t)\simeq\begin{cases}\pi^{-1}(t^2-r^2)^{-1/2}\ , & r<t\\ 0\ , & r>t\end{cases}\qquad\mu=\tfrac{3}{2}\ . \tag{84}$$

This expression shows that $P_V(r,t)$ is approximately constant for small r and diverges when r approaches t.

Fig. 13 displays $P_V(r,t)$ obtained numerically in the following way. First $\psi(k,u)$, Eq. (69), and $\Psi(k,u)$, Eq. (75) are computed using a fast Fourier procedure. Then $P_V(r,t)$, Eq. (11), is calculated through a combined numerical Fourier-Laplace inversion. For short times $t\le 100$ an exact enumeration procedure is applied. The results for $\mu=\frac{3}{2}$ are plotted for various times t. The analytical form Eq. (84) is indicated by dashed lines. Also shown is the propagator obtained from the iterated map Eq. (66) for $z=3$. The parameter ϵ was set to be $\epsilon=10^{-6}$ and averages were taken over 10^{10} iterations. The agreement between the velocity model and the map curves is remarkable. In both cases the propagator is plotted in the scaling representation.

Equations (82) to (84) should be contrasted with the corresponding $\mu=\frac{3}{2}$ form of the jump model

$$P_J(k,u)\simeq 2/\{u^{1/2}[(u+ik)^{1/2}+(u-ik)^{1/2}]\}\ , \tag{85}$$

whose asymptotic behavior is given in Eq. (80). Fig. 14 describes the behavior of $P_J(r,t)$ for $\mu=\frac{3}{2}$ calculated in the same way as $P_V(r,t)$. The difference between the jump model and the velocity model is evident and pronounced in this case. Here again the curves are plotted in the scaling representation.

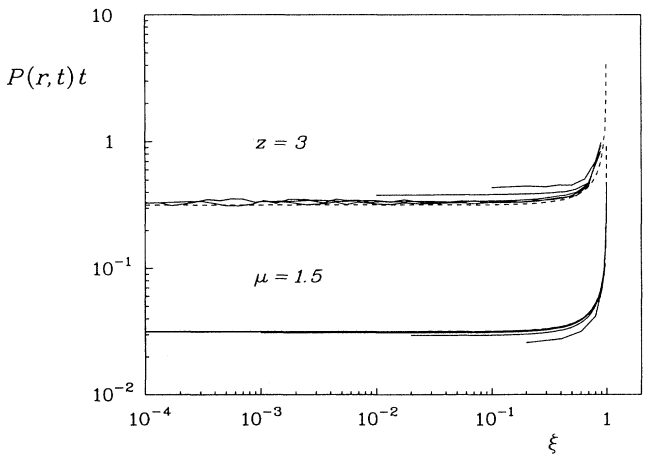

FIG. 13. Propagator $P(r,t)$ in the ballistic-type regime. The upper curves are the results of the iterated map Eq. (66) for $z=3$ and for times $t=10$, 10^2, 10^3, 10^4, and 10^5. The lower curves indicate the numerical results of $P_V(r,t)$ for $\mu=1.5$ and for the same sequence of times, shifted vertically by an order of magnitude. The broken lines give the analytical asymptotic form Eq. (84). The results are plotted in the scaling representation, the scaling variable being $\xi=r/t$.

In the second regime $2<\mu<3$ we find that to leading order the Fourier-Laplace form is the same for the jump model and for the velocity model and is given by [14]

$$P_{J,V}(k,u)=(u+\tilde{c}|k|^{\mu-1}/c_1)^{-1}\ , \tag{86}$$

where the constant is again $\tilde{c}=c_\mu\cos[\pi(\mu-1)/2]$. The Laplace inversion gives the familiar expression

$$P_{J,V}(k,t)=\exp(-\tilde{c}t|k|^{\mu-1}/c_1)\ , \tag{87}$$

which describes the Lévy distribution. From the relationship between t and k we expect a scaling behavior. The Fourier inversion can be calculated individually for the small and large r expansions [9,14]. The short-range expansion gives a Gaussian, while the long-range expansion leads to a power-law decay:

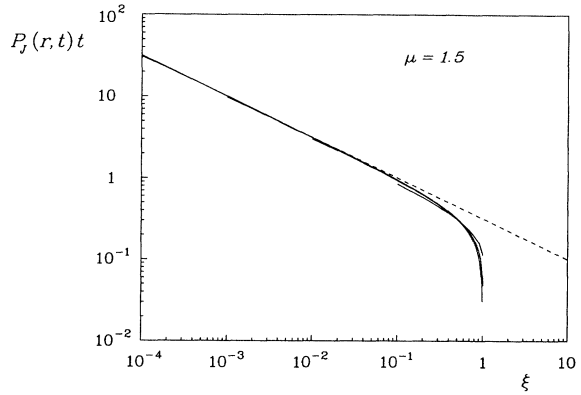

FIG. 14. Propagator of the jump model $P_J(r,t)$ in the ballistic-type regime for $\mu=1.5$ and for times $t=10$, 10^2, 10^3, 10^4, and 10^5. The broken line indicates the theoretical asymptotic form, Eq. (80). The results are plotted in the scaling representation, the scaling variables being $\xi=r/t$.

$$P_{J,V}(r,t)\simeq\begin{cases}a_0 t^{1/(1-\mu)}\exp[-a_1(r/t^{1/(\mu-1)})^2]\ , & \text{for small } r\\ bt^{1/(1-\mu)}(t^{1/(\mu-1)}/r)^\mu\ , & \text{for large } r\ ,\end{cases} \tag{88}$$

with

$$a_0=\Gamma(\mu/\mu-1)/[\pi(\tilde{c}/c_1)^{1/(\mu-1)}]\ , \tag{89a}$$

$$a_1=\Gamma(3/\mu-1)/[2\Gamma(1/\mu-1)(\tilde{c}/c_1)^{2/(\mu-1)}]\ , \tag{89b}$$

$$b=1/[2\xi(\mu-1)]\ . \tag{89c}$$

Figures 15 and 16 compare $P_V(r,t)$ and $P_J(r,t)$ in this intermediate regime. The same numerical procedure was applied as in Figs. 13 and 14, but ϵ was set to zero. In Fig. 15 we monitor $P_V(r,t)$ for the velocity model and the corresponding map-generated propagator for $z=\frac{5}{3}$. The resemblance is very good. The propagator in the jump model $P_J(r,t)$ agrees with the propagator in the velocity model $P_V(r,t)$ in the central part but deviates at the wing part.

Collecting the results in the μ range $1<\mu<3$ we can introduce the following scaling function already used in Figs. 13–16:

$$P_{J,V}(r,t)=f_{J,V}(\xi)/\tau\ ,\quad \xi=|r|/\tau\ , \tag{90}$$

with

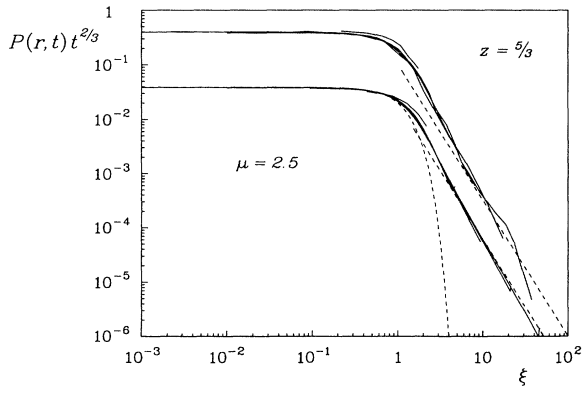

FIG. 15. Same as Fig. 13 but in the intermediate enhanced diffusion regime. The upper curves are the results of the iterated map for $z=\frac{5}{3}$. The theoretical slope for large ξ is indicated by a broken line. The lower curves give $P_V(r,t)$ for $\mu=2.5$; the broken lines give the analytical asymptotic forms Eq. (88). The scaling variable is $\xi=r/t^{2/3}$.

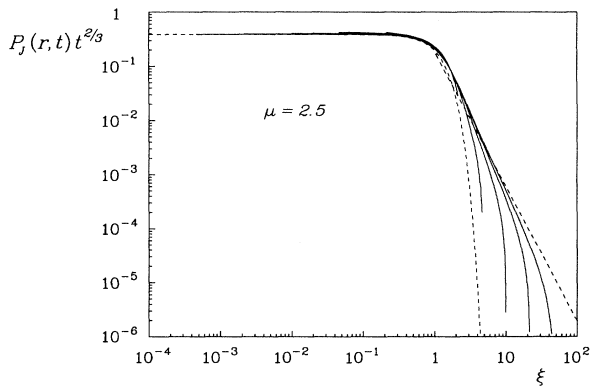

FIG. 16. Same as Fig. 14 but in the intermediate enhanced diffusion regime for $\mu=2.5$. The broken lines indicate the theoretical asymptotic form Eq. (88). The scaling variable is $\xi=r/t^{2/3}$.

$$\tau=\begin{cases} t\ , & 1<\mu<2 \\ t^{1/(\mu-1)}\ , & 2<\mu<3\ . \end{cases} \tag{91}$$

$f_{J,V}(\xi)$ denotes again the scaling functions, which for the ballistic-type regime are

$$f_J(\xi)\sim\xi^{\mu-2}\ ,\quad \xi\leq 1\ ,\quad 1<\mu<2\ , \tag{92}$$

and $f_V(\xi)$, which we have analytically only for $\mu=\frac{3}{2}$, is

$$f_V(\xi)=\pi^{-1}(1-\xi^2)^{-1/2}\ ,\quad \xi\leq 1\ ,\quad \mu=\tfrac{3}{2}\ . \tag{93}$$

For the intermediate enhanced diffusion regime $2\leq\mu<3$ we find

$$f_{J,V}(\xi)\sim\begin{cases}\exp(-a_1\xi^2)\ , & \xi<1 \\ \xi^{-\mu}\ , & 1<\xi\ ,\quad r<t \\ 0\ , & r>t\ . \end{cases} \tag{94}$$

These scaling features have been demonstrated in Figs. 13–16.

We also give the expressions for the regime $3<\mu<4$ of regular motion. Here, to leading order, the Fourier-Laplace form is given by [14]

$$P_{J,V}(k,u)=c_1/(c_1u+c_2k^2-\bar{c}|k|^{\mu-1})\ , \tag{95}$$

where again $\bar{c}=c_\mu\cos[\pi(\mu-1)/2]$. The Laplace inversion yields

$$P_{J,V}(k,t)=\exp[-t(c_2k^2-\bar{c}|k|^{\mu-1})/c_1]\ . \tag{96}$$

In this expression t and k are related to each other in two different ways and therefore there is no unique scaling through the whole range. For small r the $|k|^{\mu-1}$ term can be disregarded and one obtains a Gaussian while for large r the $|k|^{\mu-1}$ term dominates and gives rise for a power-law decay. We obtain

$$P_{J,V}(r,t)\simeq\begin{cases}a_0t^{-1/2}\exp(-a_1r^2/t)\ , & \text{for small } r \\ bt/r^\mu\ , & \text{for large } r\ , \end{cases} \tag{97}$$

with

$$a_0=[\zeta(\mu-2)/\pi\zeta(\mu-1)]^{1/2}\ , \tag{98a}$$

$$a_1=\zeta(\mu-1)/[2\zeta(\mu-2)]\ , \tag{98b}$$

$$b=1/[2\zeta(\mu-1)]\ . \tag{98c}$$

Apparently, scaling is violated by the large r power-law decay. Figs. 17 and 18 describe the propagators in the regular regime. Again the velocity model is closer to the map results Fig. 17 than the jump model Fig. 18.

We close this section by a remark on the scaling variable ξ. In order to determine ξ one may generally consider the mean-squared displacement Eq. (1) to obtain a length-time relationship and may then write

$$\xi=\frac{r}{\langle r^2(t)\rangle^{1/2}}\sim\frac{r}{t^{\alpha/2}}\ . \tag{99}$$

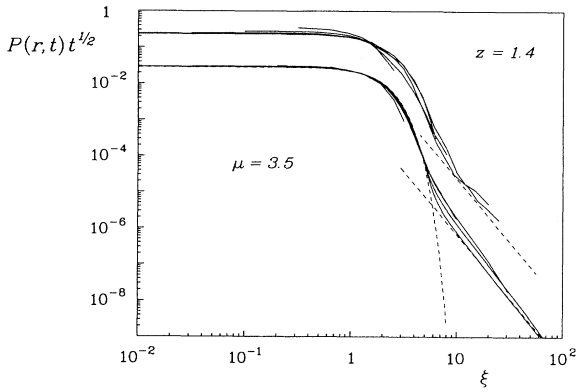

FIG. 17. Same as Fig. 13 but in the regular diffusion regime. The upper curves are the results of the iterated map for $z=1.4$. The theoretical slope for large ξ is indicated by a broken line. The lower curves depict $P_V(r,t)$ for $\mu=3.5$. The broken lines give the Gaussian behavior for $\xi\lesssim 1$, Eq. (97), and the power law bt/r^μ, $t=10^5$ for $\xi>1$, respectively. The scaling variable is $\xi=r/t^{1/2}$.

In this paper we demonstrated that Eq. (99) is not obeyed in all cases. While for the dispersive motion Eq. (99) holds, as is seen from Eqs. (41) and (57), in the intermediate enhanced diffusion regime $2<\mu<3$, expression (99) is violated. Simply, from Eq. (78) we have $\langle r^2_{J,V}(r,t)\rangle\sim t^{4-\mu}$, which does not concur with the scaling variable of Eqs. (90) and (91) $\xi=|r|/t^{1/(\mu-1)}$. Interestingly, this fact coincides with the observation that the "rule of thumb" which relates the autocorrelation function and the mean-squared displacement to each other,

$$P_0(t)\sim\frac{1}{\langle r^2(t)\rangle^{1/2}}\ , \tag{100}$$

is not obeyed in the same situation, i.e., for $2<\mu<3$ [14].

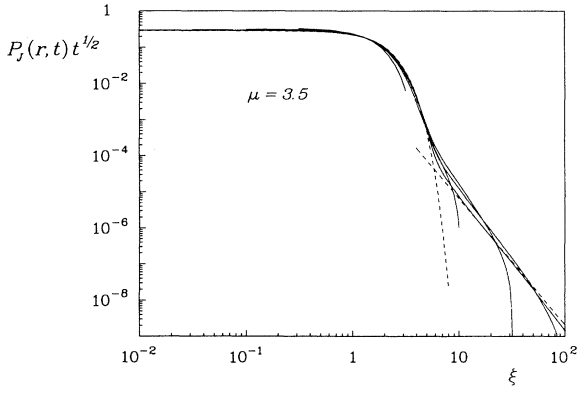

FIG. 18. Same as Fig. 14 but in the regular diffusion regime for $\mu=3.5$. The broken lines indicate the theoretical asymptotic forms Eq. (97). The scaling variable is $\xi=r/t^{1/2}$. As in Fig. 17 the broken lines give the Gaussian behavior for $\xi\lesssim 1$, Eq. (97), and the power law bt/r^μ, $t=10^5$ for $\xi>1$, respectively. The scaling variable is $\xi=r/t^{1/2}$.

V. CONCLUSIONS

In summary we have introduced and analyzed CTRW-based models that lead to anomalous diffusion. We have distinguished between the jump model and the velocity model and compared their corresponding properties. We have concentrated on the propagator $P(r,t)$ and we have confirmed previous findings on the mean-squared displacement. When tested against maps that generate anomalous behavior we find that (i) the jump model provides a good description of the dispersive motion obtained from the map in Eq. (34), and (ii) there is an excellent agreement between the properties of enhanced diffusion derived from the map in Eq. (66) and the velocity model.

Continuous-time random walks offer an effective probabilistic means to describe anomalous diffusion in deterministic systems. Both the dispersive and the enhanced cases emerge naturally either from the jump model or from the Lévy walk velocity model.

ACKNOWLEDGMENTS

We thank Professor A. Blumen, Professor K. Dressler, Dr. R. Stoop, and G. Poupart for helpful discussions and Ms. E. Warda and F. Weber for technical assistance. J. K. thanks the ETH for the hospitality during the time this work was carried out. A grant for computer time from the Rechenzentrum der ETH-Zürich is gratefully acknowledged.

[1] H. Scher and E. W. Montroll, Phys. Rev. B **12**, 2455 (1975).
[2] M. F. Shlesinger, J. Klafter, and Y. M. Wong, J. Stat. Phys. **27**, 499 (1982).
[3] G. H. Weiss and R. J. Rubin, Adv. Chem. Phys. **52**, 363 (1983).
[4] S. Havlin and D. Ben Avraham, Adv. Phys. **36**, 695 (1987).
[5] J. W. Haus and K. W. Kehr, Phys. Rep. **150**, 263 (1987).
[6] J.-P. Bouchaud and A. Georges, Phys. Rep. **195**, 127 (1990).
[7] A. Blumen, J. Klafter, and G. Zumofen in *Optical Spectroscopy of Glasses*, edited by I. Zschokke (Reidel, Dordrecht, 1986), p. 199.
[8] G. Zumofen, J. Klafter, and A. Blumen, J. Stat. Phys. **65**, 991 (1991).
[9] M. Araujo, S. Havlin, G. H. Weiss, and H. E. Stanley, Phys. Rev. A **43**, 5207 (1991).
[10] M. F. Shlesinger and J. Klafter, Phys. Rev. Lett. **54**, 2551 (1985).
[11] M. F. Shlesinger and J. Klafter, in *Transport and Relaxation in Random Materials*, edited by J. Klafter, R. J. Rubin, and M. F. Shlesinger (World Scientific, Singapore, 1986).
[12] J. Klafter, A. Blumen, and M. F. Shlesinger, Phys. Rev. A **35**, 3081 (1987).
[13] R. C. Ball, S. Havlin, and G. H. Weiss, J. Phys. A **20**, 4055 (1987); H. Weissman, G. H. Weiss, and S. Havlin, J. Stat. Phys. **57**, 301 (1989).
[14] G. Zumofen, J. Klafter, and A. Blumen, Chem. Phys. **146**, 433 (1990).
[15] P. Manneville, J. Phys. (Paris) **41**, 1235 (1980).
[16] J. I. Hirsch, B. A. Huberman, and D. J. Scalapino, Phys. Rev. A **25**, 519 (1982).
[17] T. Geisel and S. Thomae, Phys. Rev. Lett. **52**, 1936 (1984).
[18] T. Geisel, J. Nierwetberg, and A. Zacherl, Phys. Rev. Lett. **54**, 616 (1985).
[19] A. S. Pikovsky, Phys. Rev. A **43**, 3146 (1991).
[20] I. S. Aranson, M. I. Rabinovich, and L. Sh. Tsimring, Phys. Lett. A **151**, 523 (1990).
[21] X.-J. Wang, Phys. Rev. A **45**, 8407 (1992); R. N. Mantegna, J. Stat. Phys. (to be published).
[22] M. F. Shlesinger, B. West, and J. Klafter, Phys. Rev. Lett. **58**, 1100 (1987).
[23] M. F. Shlesinger and J. Klafter, J. Phys. Chem. **93**, 7023 (1989).
[24] J. Masoliver, K. Lindenberg, and G. H. Weiss, Physica A **157**, 891 (1989).
[25] G. Zumofen, A. Blumen, J. Klafter, and M. F. Shlesinger, J. Stat. Phys. **54**, 1519 (1989).
[26] S. Grossmann and H. Fujisaka, Phys. Rev. A **26**, 1779 (1982).
[27] H. G. Schuster, *Deterministic Chaos: An Introduction* (Physik Verlag, Weinheim, 1984).
[28] W. Feller, *An Introduction to Probability Theory and Its Application* (Wiley, New York, 1971), Vol. II.
[29] J. K. E. Tunaley, J. Stat. Phys. **11**, 397 (1974).